



# Accretion-modified Stars in Accretion Disks of Active Galactic Nuclei: Gravitational-wave Bursts and Electromagnetic Counterparts from Merging Stellar Black Hole Binaries

Jian-Min Wang<sup>1,2,3</sup> , Jun-Rong Liu<sup>1,2</sup>, Luis C. Ho<sup>4,5</sup> , Yan-Rong Li<sup>1</sup> , and Pu Du<sup>1</sup> 

<sup>1</sup> Key Laboratory for Particle Astrophysics, Institute of High Energy Physics, Chinese Academy of Sciences, 19B Yuquan Road, Beijing 100049, People's Republic of China; [wangjm@ihep.ac.cn](mailto:wangjm@ihep.ac.cn)

<sup>2</sup> School of Astronomy and Space Sciences, University of Chinese Academy of Sciences, 19A Yuquan Road, Beijing 100049, People's Republic of China

<sup>3</sup> National Astronomical Observatory of China, 20A Datun Road, Beijing 100020, People's Republic of China

<sup>4</sup> Kavli Institute for Astronomy and Astrophysics, Peking University, Beijing 100871, People's Republic of China

<sup>5</sup> Department of Astronomy, School of Physics, Peking University, Beijing 100871, People's Republic of China

Received 2021 March 15; revised 2021 June 2; accepted 2021 June 13; published 2021 July 30

## Abstract

The recent advanced LIGO/Virgo detections of gravitational waves (GWs) from stellar binary black hole (BBH) mergers, in particular GW190521, which is potentially associated with a quasar, have stimulated renewed interest in active galactic nuclei as factories of merging BBHs. Compact objects evolving from massive stars are unavoidably enshrouded by a massive envelope to form accretion-modified stars (AMSs) in the dense gaseous environment of a supermassive black hole (SMBH) accretion disk. We show that most AMSs form binaries due to gravitational interaction with each other during radial migration in the SMBH disk, forming BBHs inside the AMS. When a BBH is born, its orbit is initially governed by the tidal torque of the SMBH. Bondi accretion onto a BBH at a hyper-Eddington rate naturally develops and then controls the evolution of its orbits. We find that Bondi accretion leads to efficient removal of the orbital angular momentum of the binary, whose final merger produces a GW burst. Meanwhile, the Blandford–Znajek mechanism pumps the spin energy of the merged BH to produce an electromagnetic counterpart (EMC). Moreover, hyper-Eddington accretion onto the BBH develops powerful outflows and triggers a Bondi explosion, which manifests itself as an EMC of the GW burst, depending on the viscosity of the accretion flow. Thermal emission from the Bondi sphere appears as one of the EMCs. The BBHs radiate GWs with frequencies of  $\sim 10^2$  Hz, which are accessible to LIGO.

*Unified Astronomy Thesaurus concepts:* Active galactic nuclei (16); Supermassive black holes (1663)

## 1. Introduction

The outer parts of the accretion disks of supermassive black holes (SMBHs) in active galactic nuclei (AGNs) host many poorly understood, complicated processes. Star formation is unavoidable in these regions because of self-gravity (Paczynski 1978; Kolykhalov & Sunyaev 1980; Shlosman & Begelman 1989; Collin & Zahn 1999; Goodman 2003; Goodman & Tan 2004; Collin & Zahn 2008), producing compact stellar remnants from the rapid evolution of massive stars (Artymowicz et al. 1993; Cheng & Wang 1999; Cantiello et al. 2021; Grishin et al. 2021; Moranchel-Basurto et al. 2021; Wang et al. 2021). Stellar evolution rapidly releases metals into the outer parts of the self-gravitating (SG) disk (Wang et al. 2010, 2011, 2012), offering an explanation for the supersolar metallicities observed in AGNs across cosmic time (Hamann & Ferland 1999; Warner et al. 2003; Nagao et al. 2006; Shin et al. 2013; Du & Wang 2014). Interestingly, quasiperiodic ejections have been found in normal galaxies by eROSITA (Arcodia et al. 2021), implying that stellar-mass black holes (BHs) do reside around SMBHs in galactic centers. Compact objects form binaries in the very dense gaseous environment of SMBH disks, leading to  $\gamma$ -ray and gravitational-wave (GW) bursts from galactic nuclear regions (Cheng & Wang 1999). The detection by Advanced LIGO/Virgo of GWs from the mergers of stellar binary BHs (BBHs; e.g., Abbott et al. 2016a, 2016b, 2017) has renewed theoretical interest in this problem (Bartos et al. 2017; McKernan et al. 2019, 2020; Yang et al. 2019; Gröbner et al. 2020; Samsing et al. 2020; Secunda et al. 2020; Tanaga et al. 2020; Yang et al. 2020; Kaaz et al. 2021;

Li et al. 2021). The GW190521 event has garnered special attention, not only because of the large masses of the two constituent BHs (85 and 66  $M_{\odot}$ ; Abbott et al. 2020) but also because the event was potentially hosted by the quasar SDSS J1249+3449 (Graham et al. 2020; Palmese et al. 2021). Quasars and AGNs could be natural factories of high stellar mass BBHs efficiently formed in situ in SMBH disks.

Compact objects deeply enveloped by the extremely dense gas of the SMBH disk form a new kind of stellar population. Since their fates are modified by accretion from the massive envelope, we call them accretion-modified stars (AMSs). This general terminology covers a wide range of possible cores, ranging from main-sequence stars (Cantiello et al. 2021), to white dwarfs, to neutron stars, to BHs. The massive envelope of an AMS generally is associated with inflow from the Bondi accretion (Bondi 1952). It should be noted that AMSs are different from Thorne–Żytkow objects (Thorne & Żytkow 1975, 1977), not only in terms of their core, which consists of a neutron star, but also in terms of the physics of their massive envelope. As discussed in Wang et al. (2021; see also Section 2.1), AMS BHs are fed by hyper-Eddington accretion<sup>6</sup> with rates reaching up to  $10^{9-10} L_{\text{Edd}}/c^2$  for  $10-10^2 M_{\odot}$  BHs, where  $L_{\text{Edd}}$  is the Eddington luminosity and  $c$  is the speed of light. Such an accretion rate is much higher than the usual regime of slim accretion disks (Abramowicz et al. 1988; Wang & Zhou 1999). Hyper-Eddington accretion develops powerful outflows (e.g.,

<sup>6</sup> Usually when accretion rates exceed  $(10^3 \sim 10^4) L_{\text{Edd}}/c^2$ , super-Eddington accretion is usually called hyper-Eddington accretion (e.g., Takeo et al. 2020).

Takeo et al. 2020), which have a profound effect on the evolution of AMSs. As described in Wang et al. (2021), the outflows in AMSs are so strong that they can halt the accretion. The cumulative kinetic energy of the outflows drives an explosion. We call it a Bondi explosion, which in a typical quasar manifests itself as a slow transient in the radio, optical-UV, soft X-ray, and  $\gamma$ -ray bands with an occurrence rate of  $\sim 1 \text{ yr}^{-1}$  (see Equation (24) in Wang et al. 2021). On the other hand, AMSs trapped in an SMBH disk migrate radially with the accreting gas and gravitationally interact with each other if they experience close encounters over several orbital periods. This results in the formation of AMS binaries, giving rise to additional phenomena such as GW bursts.

This paper explores the formation of AMS binaries as an unavoidable consequence in SMBH disks. The orbits of the binaries evolve through several phases until their final merger generates a GW burst. Newly born BHs from the mergers are rotating very fast due to orbital angular momentum (AM). Therefore, three kinds of electromagnetic counterparts (EMCs) are considered due to (1) Blandford–Znajek (BZ) power from the spin of the merged BHs (Blandford & Znajek 1977), (2) thermal emission from a Bondi sphere, and (3) nonthermal emission from a Bondi explosion of AMSs with BBHs. They have very different timescales for BHs of  $100 M_\odot$ . The AGNs could be a factory of GW bursts.

The paper is organized as follows. In Section 2, the formation of BBHs is investigated based on the properties of the AMSs, and their formation rates are derived analytically. We study the evolution of the binaries in Section 3, in particular the observational appearance of EMCs of GW bursts when the binaries merge. Three kinds of EMCs driven by different mechanisms could appear as transients from radio to  $\gamma$ -rays. We draw conclusions in Section 4.

## 2. Formation of Binary AMSs

### 2.1. Two Types of AMS

Compact objects will be formed through rapid evolution of massive stars in SMBH disks, which originate either from captures of stars from nuclear star clusters (Artymowicz et al. 1993; Cheng & Wang 1999; Cantiello et al. 2021) or star formation in the SG disks (Collin & Zahn 1999, 2008; Goodman 2003; Wang et al. 2010, 2011, 2012). In this paper, we focus on AMS BHs, whose properties depend on the mass density of the SMBH disks. Since the SG region of AGN accretion disks is still poorly understood, we continue to use the solution of the outer part of the standard accretion disk as the characteristic structure for discussions of AMSs and related issues. The half-thickness, density, midplane temperature, and radial velocity of the SMBH disk are

$$\begin{cases} H = 4.3 \times 10^{14} \alpha_{0.1}^{-1/10} M_8^{9/10} \mathcal{M}^{3/20} r_4^{9/8} \text{ cm}, \\ \rho_d = 6.9 \times 10^{-11} (\alpha_{0.1} M_8)^{-7/10} \mathcal{M}^{11/20} r_4^{-15/8} \text{ g cm}^{-3}, \\ T_c = 4.6 \times 10^3 (\alpha_{0.1} M_8)^{-1/5} \mathcal{M}^{3/10} r_4^{-3/4} \text{ K}, \\ v_r = 2.6 \times 10^2 \alpha_{0.1}^{4/5} M_8^{-1/5} \mathcal{M}^{3/10} r_4^{-1/4} \text{ cm s}^{-1}, \end{cases} \quad (1)$$

respectively (e.g., Kato et al. 2008). Here the dimensionless quantities are the viscosity parameter  $\alpha_{0.1} = \alpha/0.1$ , the gravitational radius of the SMBH disk to that of the SMBH  $r_4 = R/10^4 R_g$ , the gravitational radius  $R_g = GM_*/c^2$ , and the

gravitational constant  $G$ , and  $M_8 = M_*/10^8 M_\odot$  is the central SMBH mass in units of  $10^8 M_\odot$ . The dimensionless accretion rate of the central SMBH is defined by  $\mathcal{M} = \dot{M}_*/\dot{M}_{\text{Edd}}$ , where  $\dot{M}_{\text{Edd}} = L_{\text{Edd}} c^{-2}$  is the Eddington rate, with the Eddington luminosity  $L_{\text{Edd}} = 1.3 \times 10^{46} M_8 \text{ erg s}^{-1}$ , and  $\dot{M}_*$  is the accretion rate of the central SMBH. The parameter (Toomre 1964), defined as  $Q = \Omega_K c_s / \pi G \rho_d H$ , describes the disk self-gravity, where  $c_s$  is the local sound speed of the disk ( $c_s \approx 15.7 T_4^{1/2} \text{ km s}^{-1}$ ), and  $\Omega_K = \sqrt{GM_*/R^3}$ . The disk becomes SG beyond a critical radius where  $Q = 1$ , which is given by  $R_{\text{SG}}/R_g = 1.2 \times 10^3 \alpha_{0.1}^{28/45} M_8^{-52/45} \mathcal{M}^{-22/45}$ . We consider AMSs in the region beyond  $R_{\text{SG}}$ . As shown by Wang et al. (2021), most AMSs are trapped by and corotate with the gas in the SMBH disk. The AMS BHs undergo episodic hyper-Eddington accretion driven by powerful outflows, leading to a Bondi explosion and maintaining very low-level accretion onto the BHs during every episode. The AMS BHs with hyper-Eddington and low-accretion rates are denoted as type I and type II AMSs. The basic properties of type I AMSs can be estimated from the Bondi accretion of cold gas in the SMBH disk, as described in Wang et al. (2021) and below.

However, the BHs are still accreting from the hot, postshock gas in the cavity of the SMBH disk after the Bondi explosion. The hot gas in the cavity determines the orbital evolution of the BBH. As shown in Wang et al. (2021; see Equation (16)), the cavity radius

$$R_{\text{exp}} = 9.0 \times 10^{15} E_{52}^{1/4} \alpha_{0.1}^{1/5} M_8^{9/20} \mathcal{M}^{-7/40} r_4^{15/16} \text{ cm}, \quad (2)$$

where  $E_{52} = E_{\text{out}}/10^{52} \text{ erg}$  is the kinetic energy of the outflow from the hyper-Eddington accretion of type I AMSs. The temperature of the shock-swept medium is

$$T_{\text{cav}} \approx \frac{2(\Gamma_{\text{ad}} - 1)m_{\text{prot}}}{(1 + \Gamma_{\text{ad}})^2 k} V_{\text{exp}}^2 = 2.3 \times 10^{11} V_{\text{exp},5}^2 \text{ K}, \quad (3)$$

where  $V_{\text{exp},5} = V_{\text{exp}}/10^5 \text{ km s}^{-1}$ ,  $m_{\text{prot}}$  is the mass of the proton,  $k$  is the Boltzmann constant, and we take the adiabatic index  $\Gamma_{\text{ad}} = 5/3$ . Since the vertical direction is open, most of the gas in the cavity will escape from the SMBH disk. In order to estimate the gas density of the cavity, we use the pressure balance between the cavity and the cold disk,

$$n_{\text{cav}} = \frac{n_d T_c}{T_{\text{cav}}} = 4.4 \times 10^6 n_{d,14} T_{d,4} V_{\text{exp},5}^{-2} \text{ cm}^{-3}, \quad (4)$$

where  $n_{d,14} = n_d/10^{14} \text{ cm}^{-3}$  and  $T_{c,4} = T_c/10^4 \text{ K}$  are the number density and temperature of the SMBH disk, respectively, which allow us to estimate the accretion rate of the type II AMSs and their mass. It should be noted that the cooling timescale of  $t_{\text{ff}} \approx 10^3 T_{11}^{1/2} n_6^{-1} \text{ yr}$  is comparable with the rejuvenation timescale of type I AMSs (see Equation 8), where  $T_{11} = T_{\text{cav}}/10^{11} \text{ K}$  and  $n_6 = n_{\text{cav}}/10^6 \text{ cm}^{-3}$ . The Bondi accretion rate can be expressed simply by  $\dot{M}_{\text{Bon}} = 4\pi G^2 m_*^2 \rho_d / c_s^3$  for AMSs of both types but with different surrounding density and temperature, where  $m_*$  is the AMS BH mass (i.e.,  $m_p$  and  $m_s$ ). In this paper, we give characteristic values of the AMS for BHs with  $10^2 M_\odot$  for a

brief application to GW190521. Its dimensionless rates are

$$\begin{aligned} \dot{m}_{\text{Bon}} &= \frac{\dot{M}_{\text{Bon}}}{\dot{M}_{\text{Edd}}} \\ &\approx \begin{cases} 8.9 \times 10^9 m_2 (\alpha_{0,1} M_8)^{-2/5} \mathcal{M}^{1/10} r_4^{-3/4} & \text{(type I AMS),} \\ 6.3 \times 10^{-9} m_2 n_{\text{cav},7} V_{\text{exp},5}^{-3} & \text{(type II AMS).} \end{cases} \end{aligned} \quad (5)$$

where  $m_2 = m_*/10^2 M_\odot$  and  $n_{\text{cav},7} = n_{\text{cav}}/10^7 \text{ cm}^{-3}$ . The Bondi radius of type I AMSs given by  $R_{\text{Bon}} = Gm_*/c_s^2$ , however, is limited by the tidal force of the SMBH. For  $m_* = 10^2 M_\odot$ , we find the Bondi radius  $R_{\text{Bon}} = 1.2 \times 10^{16} m_2 (\alpha_{0,1} M_8)^{1/5} \mathcal{M}^{-3/10} r_4^{3/4} \text{ cm}$ , which is about 10 times the thickness of the SMBH disk, and thus have a tidal-limited radius

$$R_{\text{Bon}} = \begin{cases} H & \text{(type I AMS),} \\ R_{\text{exp}} & \text{(type II AMS).} \end{cases} \quad (6)$$

The Bondi sphere, limited by the tidal force of the SMBH, has the maximal height of the SMBH disk. Here only the sound speed appears in the expression for the Bondi accretion rate; the relative velocity between the BH and SMBH disk is neglected because of corotation (see Equation (7) in Wang et al. 2021). Moreover, separations of the binary AMSs are much smaller than the Bondi radius when the relative velocities of the two BHs are larger than the sound speed of the SMBH disks. Viscosity very efficiently dissipates the orbital AM of the formed BBHs (see Equation (17)). The validity of the Bondi accretion approximation is guaranteed by  $R_{\text{Bon}} \ll R_\rho$ , where  $R_\rho = |d \ln \rho_d / dR|^{-1} \approx R$  (i.e., e-folding variations of the disk density over  $R_\rho$ ) is the density scale of the SMBH disk. Since the Bondi accretion of a type I AMS is hyper-Eddington, powerful outflows develop from the slim accretion disk (Ohsuga et al. 2005; Kitaki et al. 2018). Radiative feedback, which operates in super-Eddington accretion (Wang et al. 2006; Milosavljević et al. 2009a, 2009b), may be dominated by outflows in hyper-Eddington accretion (Takeo et al. 2020). In the present context, we consider powerful outflows as the dominant mechanism that drives episodic accretion of the AMS BHs (Wang et al. 2021).

The Bondi mass, which is defined as the gas mass within the Bondi radius, can be approximated by

$$\begin{aligned} M_{\text{Bon}} &= \frac{4\pi}{3} R_{\text{Bon}}^3 (\rho_d, \rho_{\text{cav}}) \\ &= \begin{cases} 2.1 \times 10^2 M_\odot \rho_{10} H_{15}^3 & \text{(type IAMS),} \\ 3.5 \times 10^{-6} M_\odot R_{\text{Bon},15}^3 n_6 & \text{(type IIAMS),} \end{cases} \end{aligned} \quad (7)$$

where  $\rho_{10} = \rho_d/10^{-10} \text{ g cm}^{-3}$ ,  $H_{15} = H/10^{15} \text{ cm}$ , and  $R_{\text{Bon},15} = R_{\text{Bon}}/10^{15} \text{ cm}$ . The tidal force limits the size of the Bondi sphere and hence its mass similar to that of a  $10 M_\odot$  BH (Wang et al. 2021). Without the tidal limit, the Bondi sphere of a  $100 M_\odot$  BH will be  $10^2$  times that given by Equation (7). A type II AMS has a much lower accretion rate and mass compared to its type I counterpart. Type II AMSs are expected to contain an advection-dominated accretion flow (Narayan & Yi 1994) and are generally too faint to be observed. On the other hand, the cavity formed by the Bondi explosion is replenished by the infall of gas from the

SMBH disk, rejuvenating the AMS on a timescale of

$$t_{\text{rej}} = \frac{R_{\text{exp}}}{c_s} = 267.0 \alpha_{0,1}^{3/10} M_8^{11/20} \mathcal{M}^{-13/40} r_4^{21/16} E_{52}^{1/4} \text{ yr.} \quad (8)$$

We then have the duty cycle of hyper-Eddington accretion episodes of the AMS BHs,  $\delta_* \approx 5.3 \times 10^{-5}$ , namely, the ratio of hyper-Eddington accretion time to the rejuvenation time (see details in Wang et al. 2021).

Here it is helpful to distinguish between two kinds of hyperaccreting cases. Hyper-Eddington accretion onto the BHs produces nonrelativistic but powerful outflows, or mildly moving blobs from the choked jet if the BH is rotating maximally. This differs from the case of long  $\gamma$ -ray bursts (Woosley 1993), whose highly relativistic jets are produced by accretion of neutrons (also some stellar envelope gas) onto BHs at hyper-Eddington rates. The cores of massive stars, where neutrino cooling dominates, typically supply an accretion rate of  $1 M_\odot \text{ s}^{-1} \approx 10^{15} \dot{M}_{\text{Edd}}$ . Unlike long  $\gamma$ -ray bursts, jet production could be suppressed in type I AMS BHs, despite their hyper-Eddington accretion rates. This is evidenced by the fact that AGNs with high accretion rates are usually radio-quiet (e.g., Ho 2002, 2008; Sikora et al. 2007), for jets are quenched in BHs accreting in their high, soft states (e.g., Fender et al. 2004). However, the current situation for merging BHs with  $\gtrsim 10^9 \dot{M}_{\text{Edd}}$  is uncertain based on the latest numerical simulations (Sadowski & Narayan 2015, 2016). Usually neutrino cooling, which is extremely sensitive to temperature (its rate is proportional to  $(T/10^{11} \text{ K})^9$ ), is triggered when the temperature is higher than  $10^{11} \text{ K}$  (e.g., Popham et al. 1999). However, accretion rates of  $10^9$ – $10^{10} \dot{M}_{\text{Edd}}$  are still not high enough to trigger neutrino cooling, since the overall temperature of a self-similar disk is only  $\lesssim 10^9 \text{ K}$  (Wang & Zhou 1999), and the temperature will be significantly lower if strong outflows are developed. Under such conditions, we expect powerful outflows (Takeo et al. 2020), which have much wider opening angles than jets.

On the other hand, strong magnetic fields play a key role in the formation of the highly relativistic jets in  $\gamma$ -ray bursts. In the same spirit, we explore the possibility that powerful relativistic jets could be produced either by the radiation pressure of super-Eddington accretion of nonrotating BHs (Sadowski & Narayan 2015) or by the BZ mechanism of fast-rotating BHs (Blandford & Znajek 1977). Considering the many uncertainties of hyper-Eddington accretion and the lack of clear observational tests, we explore both BZ-powered jets and Bondi explosions as potential mechanisms for generating an EMC.

## 2.2. Binary AMSs

Three cases of binary AMSs are possible: (1) type I+I, (2) type I+II, and (3) type II+II. Considering that the duty cycle of type I AMSs is only  $\sim 5 \times 10^{-5}$ , we expect most AMSs to be type II. While cases 1 and 2 are possible, their numbers are much smaller than those of case 3. In this paper, we only focus on the case where both members of the binary are type II AMSs, as shown in Figure 1.

Since AMSs are trapped by the SMBH disk, they migrate with the gas and form binaries through their gravitational interaction once they are sufficiently close. Given  $N$  BHs in the SMBH disk, their surface density is  $\Sigma_* = N_*/\pi R^2$ . Considering velocity differences of  $\Delta V = \Omega_K \mathcal{A}_0/2$ , AMSs will encounter

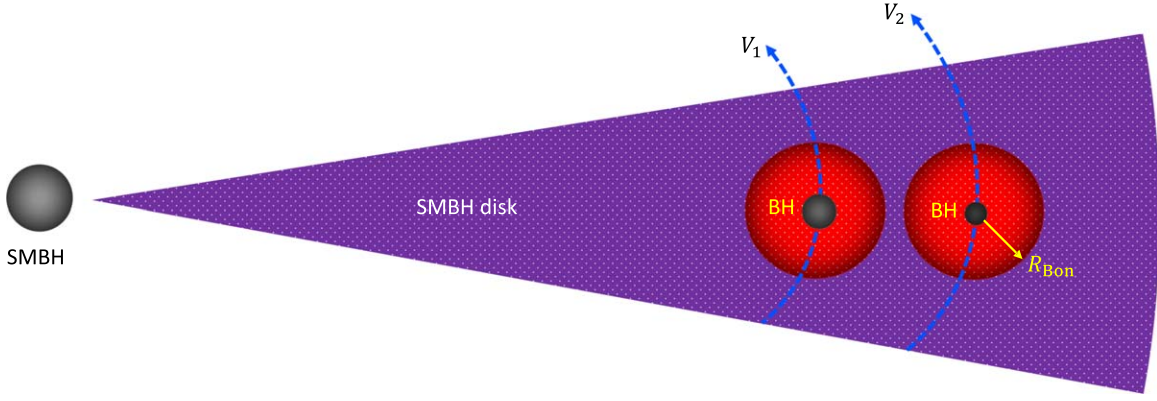


**Figure 1.** Top view of the SMBH disk. Surrounded by the SMBH disk cold gas, stellar-mass BHs form AMSs through hyper-Eddington accretion. They are denoted type I AMSs. A Bondi explosion of the AMS creates cavities with a high-temperature and low-density medium (red), but the BHs remain there and are still accreting with very low rates, forming type II AMSs. A pressure balance remains between the cavity and the cold gas of the SMBH disk. The cavities are orbiting the central SMBH with velocities  $V_1$  and  $V_2$ , respectively. The differential velocity  $|V_2 - V_1|$  determines the timescale of binary formation when they encounter after many orbits around the central SMBH. The BBHs are formed in the cavities initially appearing as type II AMSs. Subsequent evolution of the BBH orbit undergoes three different phases, as detailed in the text.

within a timescale of  $t_{\text{bin}} = 2\pi R/n \cdot \Delta V$  after many orbits around the central SMBH, where  $n = 2\pi R \mathcal{A}_0 \Sigma$  is the number of BHs in an annulus of width  $\mathcal{A}_0$ . In principle, an AMS binary can form when the gravity between the individual BHs is stronger than the tidal force of the SMBH acting on the binary. Given the tidal force  $F_{\text{tid}} = GM_* m (\mathcal{A}_0/R)/R^2$  and the gravity of the BBH  $F_{\text{bin}} = Gm^2/\mathcal{A}_0^2$ , the condition  $F_{\text{bin}} \geq F_{\text{tid}}$  places an upper limit on the distance between two AMSs,

$$a_0 = \left(\frac{m_*}{M_*}\right)^{1/3} \left(\frac{R}{r_g}\right) = 1.0 \times 10^8 M_8^{2/3} m_2^{-2/3} r_4, \quad (9)$$

where  $a_0 = \mathcal{A}_0/r_g$  and  $r_g = Gm_p/c^2$ . This condition can also be derived from the virial relation that the sum of the kinetic and potential energy of the BBH vanishes. As shown by Equation (9), the upper limit of the separation between the two BHs is much smaller than the Bondi radius. This validates the approximation of Bondi accretion onto the BBH during the orbital evolution. Moreover, the relative velocities of the two BHs are only  $\sim 30 \text{ km s}^{-1}$  initially, which is much smaller than the sound speed of the SMBH disk and cavity. The bounded BBHs remain inside a type II AMS corotating with the gas of the SMBH disk.<sup>7</sup> The appearance of GW bursts and EMCs depends on the evolution of the BBH orbit and details of its accretion history.

For simplicity, we only discuss BHs of equal mass. Once BHs enter the annulus  $R - (R - \mathcal{A}_0)$  of the SMBH disk, BBHs form nearly instantaneously compared with the AGN lifetime,  $t_{\text{AGN}} \approx R/v_r \approx 1.8 \times 10^7 \alpha_{0.1}^{-4/5} M_8^{6/5} \mathcal{M}^{-3/10} r_4^{5/4} \text{ yr}$  (from Equation (1)). For binaries formed from neighboring BHs, the timescale for BBH formation is

$$t_{\text{bin}} = \frac{4\pi}{n \cdot \Omega_K} \left(\frac{M_*}{m_*}\right)^{1/3} = 2.5 \times 10^4 N_{40}^{-1} M_8^{5/3} m_2^{-2/3} r_4^{3/2} \text{ yr} \quad (10)$$

<sup>7</sup> In the scenario of Cantiello et al. (2021), stars in the SMBH disk are from captures from a nuclear star cluster. The BHs from these stars could have different dynamics. This is beyond the scope of the present paper.

in the formation zone, with a rate from one quasar

$$\dot{N}_{\text{bin}} = \frac{n_*}{t_{\text{bin}}} \left(\frac{R}{\mathcal{A}_0}\right) = 3.2 \times 10^{-3} N_{40}^2 m_2^{2/3} M_8^{-5/3} r_4^{-3/2} \text{ yr}^{-1}, \quad (11)$$

where  $N_{40} = N/40$  from the entire SMBH disk,<sup>8</sup> and the factor  $R/\mathcal{A}_0$  is the number of formation zones. The rate in Equation (11) is an order of magnitude higher than the rate for tidal disruption events of stars in normal galactic centers (e.g., Rees 1988). The estimate of  $N$  depends on the number of massive stars in the SMBH disk, whose formation efficiency relies on the initial mass function. Here we conservatively estimate  $N$  assuming a star formation efficiency of 0.1 and a top-heavy initial mass function with a power-law index of 0.5 (see Wang et al. 2021). In this paper, we neglect AMSs composed of neutron stars, which likely undergo more complicated processes than BHs.

We note that the number of BHs in the SMBH disk could be decreased by BBH mergers. For the binary rates given by Equation (11),  $dN/dt = -\dot{N}_{\text{bin}}$  implies  $N = N_0/[1 + \pi^{-1} \Omega_K (m_*/M_*)^{2/3} N_0^0 t]$ , where  $N_0$  is the initial number of BHs. The asymptotic evolution of the number of BHs is  $N \propto t^{-1}$  when  $t \gg N_0^{-1} \pi \Omega_K^{-1} (m_*/M_*)^{-2/3}$ . Here we neglect the growth of the merging BHs. This binary rate is the maximum value for the initially given number of BHs.

### 3. Mergers of BBHs

#### 3.1. Orbital Evolution of BBHs

Differential rotation of the SMBH disk gives rise to an initial orbital AM for the binary type II AMS corotating with the disk. As shown in Figure 2, the velocities of the primary and secondary BHs relative to the center of mass are  $\Delta v_p = V_K a_p/2R$  and  $\Delta v_s = -V_K a_s/2R$ , respectively, where  $V_K = R\Omega_K$  is the Keplerian velocity,  $a_p = q\mathcal{A}_0/(1+q)$  and

<sup>8</sup> Wang et al. (2021) estimated the number of  $10 M_\odot$  BHs, but the number of  $10^2 M_\odot$  BHs is hard to estimate for a number of reasons, including uncertainties in the initial mass function of the progenitor stars and the growth of the BHs in the SMBH disk. Considering the possibility that the initial mass function in the disk might be top-heavy, we assume  $N \propto m_*^{-1}$  and have  $N_* = 40$  BHs with  $10^2 M_\odot$ .

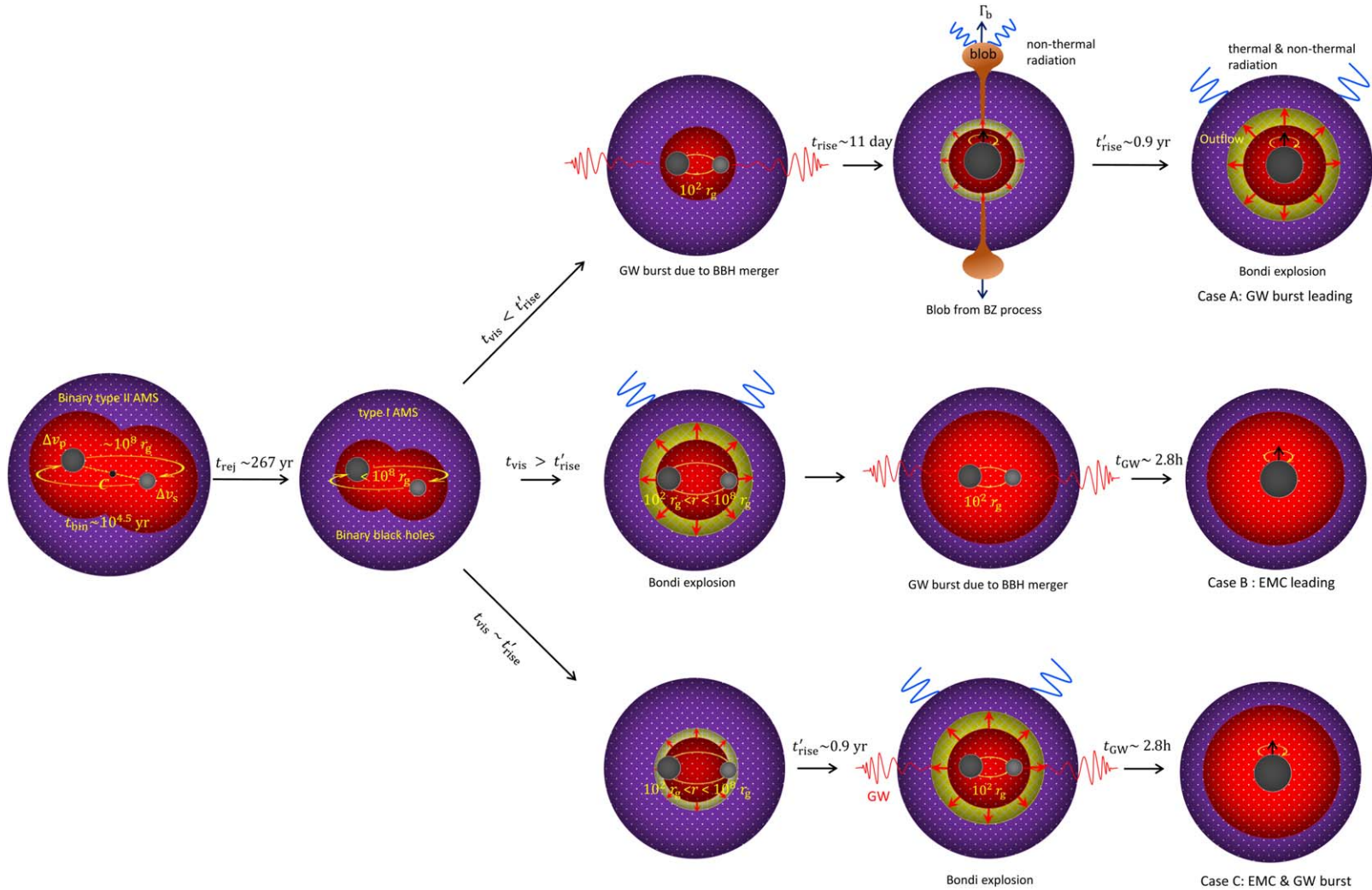


**Figure 2.** A BBH with primary mass  $m_p$ , secondary mass  $m_s$ , and center of mass  $C$  is formed while cold gas from the SMBH disk (purple) replenishes the cavity (red). All numbers of this cartoon are for  $100 M_\odot$  BHs. A type I AMS rejuvenates from a type II AMS with a timescale  $t_{\text{rej}}$ . The orbital evolution of the BBH is initially controlled by the tidal torque of the central SMBH, later by hyper-Eddington accretion, and finally by the merger of the two BHs because of a GW radiation. The spin AM of the Bondi sphere is very low because of efficient spin-down by the tidal torque of the central SMBH. Three kinds of EMCs can be generated: (1) an ejected blob moving with mildly relativistic velocity (its Lorentz factor  $\Gamma_b \sim 2$ ) by the BZ mechanism pumping the spin energy of the merged BHs, (2) thermal emission from a Bondi sphere (typically 4200 K), and (3) nonthermal emission from a Bondi explosion driven by the outflows developed from the hyper-Eddington accretion. Compared with the blob, the Bondi explosion gives rise to a slow transient as an EMC peaking in the optical bands, but nonthermal emission from the shocked gas can also arise in the radio band to energy of a few TeV. Here we stress that the three possible cases depend on the degree to which viscosity removes the orbital AM of the BBHs.

$a_s = \mathcal{A}_0/(1+q)$  are the distances of the primary and secondary BHs to the center,  $\mathcal{A}_0$  is the initial separation of the BBH, and  $q = m_s/m_p$  is the mass ratio of the binary. Here the negative sign of  $\Delta v_s$  means that the two BHs have opposite velocities in the center-of-mass frame. The initial orbital AM is then given by  $\mathcal{J}_0 = m_p V_K (\mathcal{A}_0^2/2R) q(1+q)^{-1}$ . For a BBH in Keplerian rotation, its circular orbital AM is  $\mathcal{J}_{\text{cir}} = (GA)^{1/2} m_p^{3/2} q/(1+q)^{1/2}$ , and  $\mathcal{A} = (M./m_p)(\mathcal{A}_0/R)^3 \mathcal{A}_0/4(1+q) \sim \mathcal{A}_0$  from  $\mathcal{J}_0 = \mathcal{J}_{\text{cir}}$  for  $M. = 10^8 M_\odot$ ,  $m_p = 10 M_\odot$ ,  $\mathcal{A}_0 = 10^{15}$  cm, and  $R = 10^4 R_g$  from  $\mathcal{J}_{\text{cir}} = \mathcal{J}_0$ . The initial BBHs are expected to have circular orbits. Figure 2 outlines the evolutionary track of the BBH from its birth.

The SMBH exerts a tidal torque on the BBHs given by

$$\mathcal{T}_{\text{tid}} \approx V_K^2 m_p (1+q) \left( \frac{\mathcal{A}}{R} \right)^2 \quad (12)$$

on a tidal timescale of

$$t_{\text{tid}} = \frac{\mathcal{J}_{\text{cir}}}{\mathcal{T}_{\text{tid}}} = 15.7 q(1+q)^{-3/2} a_8^{-3/2} m_2^{-1} M_8^2 r_4^3 \text{ yr}, \quad (13)$$

where  $a_8 = a/10^8$  and  $a = \mathcal{A}/r_g$ . During its orbit evolution, a type II AMS undergoes rejuvenation and accumulates gas through Bondi accretion. Compared with the rejuvenation timescale of AMSs, the tidal timescale will be longer than  $t_{\text{rej}}$  after  $a \lesssim 10^7$ . In other words, the tidal torque does not efficiently remove the orbital AM of the BBHs after a period of  $t_{\text{tid}} \sim t_{\text{rej}}$ . Since the subsequent process is much more efficient than tides, we neglect tidal effects such as the evolution of eccentricity and semimajor axis by the Kozai–Ledov mechanism (e.g., Naoz 2016). However, accretion onto the BBH should be considered (e.g., Antoni et al. 2019; Comerford et al. 2019). We approximate the accretion as if the binary were a single BH because the binary separation is much smaller than the Bondi radius. In the future, the orbital evolution of the BBH should consider accretion onto each BH.

An AMS with a single BH should have a very low spin AM. The spin AM of the Bondi sphere from the differential rotation of the SMBH disk is given by

$$\mathcal{J}_{\text{Bon}} \approx M_{\text{Bon}} V_K \frac{R_{\text{Bon}}^2}{2R}. \quad (14)$$

However, an AMS trapped in the SMBH disk will be synchronized with the orbital rotation by the tidal torque. This is just opposite to the AM of the accreted gas from the disk. Similar to Equation (12), the tidal torque exerting on the Bondi sphere,  $\mathcal{T}_{\text{tid}}^{\text{Bon}} \approx V_K^2 M_{\text{Bon}} (R_{\text{Bon}}/R)^2$ , removes the spin AM of the Bondi sphere on a timescale

$$t_{\text{tid}}^{\text{Bon}} = \frac{\mathcal{J}_{\text{Bon}}}{\mathcal{T}_{\text{tid}}^{\text{Bon}}} = 0.5 \Omega_K^{-1} = 7.8 r_4^{3/2} M_8 \text{ yr}. \quad (15)$$

This indicates that the tidal torque efficiently removes the spin AM. We thus expect that the Bondi sphere has a very low spin AM. After the tidal interaction phase with the SMBH, the BBH enters the rejuvenation phase, during which it will undergo accretion from the Bondi sphere and efficiently remove the BBH orbital AM.

Assuming that the viscosity in the Bondi sphere follows the standard  $\alpha$  prescription (Shakura & Sunyaev 1973), the torque due to viscosity is given by  $\mathcal{T}_{\text{vis}} = \alpha \rho_{\text{Bon}} c_s^2 \mathcal{V}_{\text{Bon}} = \alpha E_{\text{th}}$ ,

where  $\mathcal{V}_{\text{Bon}}$  is the volume of the Bondi sphere and  $E_{\text{th}} = \rho_{\text{Bon}} c_s^2 \mathcal{V}_{\text{Bon}}$  is the thermal energy of the sphere. Since the BBH is accreting from the sphere at a hyper-Eddington rate, powerful outflows heat the Bondi sphere with an energy

$$E_{\text{out}} = L_{\text{out}} t_a = 1.3 \times 10^{52} \eta_{0.1} f_3 m_2 \dot{m}_{10} t_{a,6} \text{ erg}, \quad (16)$$

where  $L_{\text{out}} = \eta f_a \dot{m}_{\text{Bon}} L_{\text{Edd}}$  is the kinetic energy of the outflows,  $f_a = 10^{-3} f_3$  is the fraction of the Bondi flow to fall into the BH,  $\dot{m}_{10} = \dot{m}_{\text{Bon}}/10^{10}$ ,  $\eta_{0.1} = \eta/0.1$  is the efficiency of accretion, and  $t_{a,6} = t_a/10^6$  s is the episodic accretion timescale (depending on some other parameters of the SMBH disk). We conservatively assume that the thermal energy of the Bondi sphere is  $E_{\text{th}} = \alpha E_{\text{out}} = 10^{51} \alpha_{0.1} E_{52}$  erg from the kinetic outflows. This can be justified by the role of turbulence in the thermalization of the kinetic energy of the outflows. The timescale for removing the orbital AM of the BBH is

$$t_{\text{vis}} = \frac{\mathcal{J}_{\text{cir}}}{\mathcal{T}_{\text{vis}}} = 0.28 \alpha_{0.1}^{-2} E_{52}^{-1} m_2^2 a_8^{1/2} q(1+q)^{-1/2} \text{ yr}. \quad (17)$$

It should be noted that this timescale is very sensitive to  $\alpha$ , which is quite uncertain.

After rejuvenation, the accretion rates of type I AMSs reach  $\sim 10^{9-10} L_{\text{Edd}} c^{-2}$  (see Equation 5), and powerful outflows will be developed (Ohsuga et al. 2005; Kitaki et al. 2018; Takeo et al. 2020). The outflows have a strong impact on the hyper-Eddington accretion through strong shocks heating the AMS. The accretion terminates if the temperature of the postshocked medium is higher than the virial temperature, and the hyper-Eddington accretion is thus episodic with a timescale ( $t_a$ ). See details in Wang et al. (2021). The accretion episode of the AMS, approximated by the model for a single BH, occurs on a timescale

$$t_a = \left( \frac{16\sqrt[3]{5} c^{4/3} r_g^{2/3} M_{\text{Bon}}}{9 \alpha^{2/3} L_{\text{out}}} \right)^{3/5} \\ = 4.5 \times 10^5 \eta_{0.1}^{-3/5} \alpha_{0.1}^{-2/5} f_3^{-3/5} \dot{m}_{10}^{-3/5} m_2^{-1/5} \\ \times (M_{\text{Bon},2}/2.1)^{3/5} \text{ s}, \quad (18)$$

where  $M_{\text{Bon},2} = M_{\text{Bon}}/10^2 M_\odot$ .

Subsequent evolution of the AMS with BBHs depends on the three timescales of  $t_{\text{vis}}$ ,  $t_{\text{GW}}$ , and  $t_{\text{rise}} (t'_{\text{rise}})$ , which are given by Equations (17) (19) and (26) or (32) in Section 3.3. The observational appearance of the EMCs is due to two kinds of mechanisms driven by the BZ process (depending on BH spin) and dynamics of the Bondi sphere (Equation (19)), respectively. Figure 2 shows a cartoon depicting three channels producing EMCs and GW bursts. Since the orbital evolution strongly depends on viscosity ( $\alpha$  in Equation (17)), generally, they are divided by the viscosity timescale of the Bondi sphere compared with the rise timescale of radiation from the sphere. Case A appears when the viscosity efficiently removes orbital AM, case B is inefficient, and case C is moderately efficient.

### 3.2. BBH Mergers

The initial separation of a BBH,  $\mathcal{A}_0 = 10^8 r_g$ , will be greatly reduced by an amount that depends on the AM of the rest of the hot gas within the cavity after the Bondi explosion. Eccentricity evolution is also important for GW bursts (Gröbner et al. 2020; Secunda et al. 2020), but we only take into account circular

orbits of BBHs. The GW process dominates when  $t_{\text{vis}}$  (given by Equation (17)) is longer than the timescale for the BBH to merge due to GW radiation,

$$t_{\text{GW}} = \frac{5a^4}{64q(1+q)} \left( \frac{r_g}{c} \right) \approx 2.8(a_2/1.27)^4 m_2 q^{-1} (1+q)^{-1} \text{ hr}, \quad (19)$$

where  $a_2 = a/10^2$  (Peters 1964), and the corresponding separation of the BBHs

$$a = 126.9 \alpha_{0.1}^{-4/7} q^{4/7} (1+q)^{1/7} E_{52}^{-2/7} m_2^{2/7}. \quad (20)$$

The GW frequencies are

$$f_{\text{GW}} = 56.7(1+q)^{1/2} m_2^{-1} (a/5)^{-3/2} \text{ Hz}, \quad (21)$$

which fall within the regime of LIGO. The GW bursts due to the present mechanism occur at a detectable rate of

$$\dot{R}_{\text{GW}} \approx n_q \mathcal{V}_{\text{cm}} \dot{N}_{\text{bin}} \approx 3.0 n_{q,6} \mathcal{V}_{158} \dot{N}_3 \text{ yr}^{-1}, \quad (22)$$

where  $n_{q,6} = n_q/6 \text{ Gpc}^{-3}$  is the number density of quasars (for  $z \approx 1$ ; see Richards et al. 2006),  $\mathcal{V}_{158} = \mathcal{V}_{\text{cm}}/158 \text{ Gpc}^3$  is the comoving volume within  $z=1$ , and  $\dot{N}_3 = \dot{N}_{\text{bin}}/3.2 \times 10^{-3} \text{ yr}^{-1}$  (in one quasar). Here we assume the cosmological parameters  $\Omega_m = 0.3$ ,  $\Omega_\Lambda = 0.7$ , and  $H_0 = 70 \text{ km s}^{-1} \text{ Mpc}^{-1}$ .

The LIGO-Virgo collaboration estimates a BBH merger rate of  $53.2_{-28.8}^{+58.5} \text{ Gpc}^{-3} \text{ yr}^{-1}$  for the local universe from the O1 and O2 observing runs (LIGO Scientific Collaboration & Virgo Collaboration 2019a, 2019b). This rate can be explained by BBH mergers from dense star clusters (e.g., Antonini & Perets 2012; Martinez et al. 2020). Our present BBH merger rate is lower than the detected rate by 1 order of magnitude, although the detection of GW190521 is consistent with the predictions of this paper. The present prediction is also lower than that of  $12 \text{ Gpc}^{-3} \text{ yr}^{-1}$  by Secunda et al. (2020; see their Equation (7)) and McKernan et al. (2019), but they used a BH number of  $N_* = 2 \times 10^4$ , much larger than ours. Moreover, the difference comes from the fact that the present scenario favors mergers of high-mass BBHs in the very dense environment of an SMBH disk. Mergers of BBHs less than  $10 M_\odot$  would be fainter, and their EMCs are hard to detect.

The abundance of AMSs related to GW bursts in SMBH disks can be plausibly tested by AGN variability. As predicted by Wang et al. (2021), the characteristic light curves decay as  $t^{-6/5}$ , with no intraband delays from radio to  $\gamma$ -rays. Identifying these features of AGN light curves will greatly advance our understanding of AMS physics in the SMBH disk, as well as the role they play in supplying gas to the central engine.

### 3.3. Electromagnetic Counterpart

In this subsection, we outline the characteristics of AMS emissions as EMCs of GW bursts. Emissions from the AMS depend on the details of the merged BHs and the Bondi sphere but also on the specifics of the broad-line region (BLR) of the AGNs. Except for the Bondi explosion, some energy pumped from the BH spin is released, as the AMSs must rotate very quickly from the orbital AM, whatever their spins prior to the merger (e.g., Hughes & Blandford 2003). In this paper, we explore two possible channels for generating EMCs: (1) relativistic jets from the hyper-Eddington accretion driven by a BZ mechanism pumping the rotating energy of the BHs and

(2) a Bondi explosion driven by outflows from the hyper-Eddington accretion.

#### 3.3.1. Relativistic Ejecta after BHs Merge

In the Appendix, we derive the BZ power during the accretion episode of the BH in an AMS. The BZ-powered jet is choked by the dense medium of the Bondi sphere, forming a blob as ejecta from the Bondi sphere. In this paper, we neglect the details of the choking processes in order to estimate the average Lorentz factor of the ejected blob in light of the energy equation given by  $E_{\text{BZ}} \approx E_{\text{kin}} = 2\Gamma_b \Delta M_{\text{BZ}} c^2$ , which yields

$$\Gamma_b = 1.8 E_{\text{BZ},51} R_{\text{jet},12}^{-2} R_{\text{Bon},15}^{-1} \rho_{10}, \quad (23)$$

where  $E_{\text{BZ},51} = E_{\text{BZ}}/10^{51} \text{ erg}$  is the energy pumped from the BH spin,  $E_{\text{kin}}$  is the kinetic energy of the blob,  $R_{\text{jet},12} = R_{\text{jet}}/10^{12} \text{ cm}$  is the jet radius, and  $\Delta M_{\text{BZ}} \approx \pi R_{\text{jet}}^2 R_{\text{Bon}} \rho_d \approx 1.6 \times 10^{-4} R_{\text{jet},12}^2 R_{\text{Bon},15} \rho_{10} M_\odot$  is the mass contained in the volume of the jet configuration. Here the factor 2 accounts for the double-sided nature of relativistic jets. Equation (23) shows that the ejected blobs are moving mildly relativistically, but Doppler boosting significantly enhances the luminosity by a factor of  $\Gamma_b^4$ . The initial radius of the blob is approximated by  $R_{\text{blob}}^0 \approx (R_{\text{jet}}^2 R_{\text{Bon}})^{1/3} \approx 10^{13} R_{\text{jet},12}^{2/3} R_{\text{Bon},15}^{1/3} \text{ cm}$ , corresponding to the initial optical depth of  $\tau_{\text{es}}^0 = \kappa_{\text{es}} \rho_d R_{\text{blob}}^0 = 340 \rho_{10} (R_{\text{blob}}^0/10^{13} \text{ cm})^{-2}$ , where  $\kappa_{\text{es}} = 0.34$  is the opacity of electron scattering. The total energy of the blob is composed of two components,  $E_{\text{BZ}} = E_{\text{kin}} + E_{\text{th}}$ , where  $E_{\text{th}}$  is its thermal energy. The relative strength of the two components depends on the details of the dynamics of the choked jet inside the Bondi sphere. Meanwhile, collimation supported by the cocoon of the dense surroundings keep the choked jet in the inner part of the SMBH disk (Bromberg et al. 2011; Perna et al. 2021; Zhu et al. 2021). Considering the opening angle  $\theta \approx c_s/c \approx \Gamma_b^{-1}$ , where  $c_s$  is the sound speed of the choked jet, we have  $E_{\text{kin}} \approx \Gamma_b^2 E_{\text{th}}$  when the blob is ejected outside the SMBH disk (or atmosphere of the disk). The ratio  $E_{\text{kin}}/E_{\text{th}}$  decreases with the expansion and motion of the blob as it sweeps through the BLR after it is born.

The blob undergoes three phases: (1) free expansion; (2) blast wave, when the swept medium is comparable with the mass of the blob; and (3) snowplow, when the swept mass is about  $\zeta \approx 10$ –30 times the initial mass of the blob (e.g., details in latest numerical simulations of Petruk et al. 2021). The characteristic expansion velocity of the blob is approximated by

$$\frac{V_{\text{exp}}}{c} = \begin{cases} 1 & (\text{for } t \lesssim t_c), \\ 1.0(t/t_c)^{-3/5} & (\text{for } t \gtrsim t_c). \end{cases} \quad (24)$$

Namely, the blob expands with the speed of light before  $t_c$ , and then with the Sedov velocity, where  $t_c \approx 2.9 \times 10^4 \text{ s}$  is given by  $V_{\text{exp}}/c = 1$  and  $R_c = ct_c = 8.8 \times 10^{14} \text{ cm}$ . We find that  $R_c \approx R_{\text{exp}} = (E/\rho)^{1/5} t_c^{2/5}$  (Sedov expansion) for  $E = 10^{51} \text{ erg}$  and  $\rho \approx 10^{-17} \text{ g cm}^{-3}$ . At this moment, the ejected blob has an optical depth  $\tau_{\text{es}} = \rho_{\text{blob}} \kappa_{\text{es}} R_{\text{blob}} \approx 10^{-2} \Delta M_{\text{BZ},4} R_{\text{blob},15}^{-2}$ , where  $\rho_{\text{blob}} = 3 \Delta M_{\text{BZ}}/4\pi R_{\text{blob}}^3$  is the blob density,  $\Delta M_{\text{BZ},4} = \Delta M_{\text{BZ}}/10^{-4} M_\odot$ , and  $R_{\text{blob},15} = R_{\text{blob}}/10^{15} \text{ cm}$ . The swept mass for

$t \gtrsim t_c$  is given by

$$\frac{\Delta M_{\text{BLR}}}{M_{\odot}} \approx 2.4 \times 10^{-5} \left( \frac{t}{t_c} \right)^{6/5}. \quad (25)$$

As shown by numerical simulations, the kinetic energy can be converted into thermal energy when the swept mass is about  $\zeta = 10\text{--}30$  times the mass of the blob (e.g., Petruk et al. 2021). The luminosity peaks because no significant energy is supplied by the conversion of the kinetic energy to the blob, as thermal energy drives the expansion. For  $\Delta M_{\text{BLR}} = 15 \zeta_{15} \Delta M_{\text{BZ}}$ , we have a rise timescale of

$$t_{\text{rise}} \approx 10.7 \zeta_{15}^{5/6} \Delta M_{\text{BZ},4}^{5/6} n_{\text{BLR},7}^{-1/3} E_{51}^{-1/2} \text{ days}, \quad (26)$$

where  $\zeta_{15} = \zeta/15$ , and  $n_{\text{BLR},7} = n_{\text{BLR}}/10^7 \text{ cm}^{-3}$  is the number density of the BLR. The observed luminosity of the blob is

$$L_{\text{peak}}^{\text{BZ}} \approx \Gamma_b^4 \xi L_{\text{BZ}} = 3.2 \times 10^{45} \Gamma_{2,\xi_{0.1}}^4 f_3 \dot{m}_{10} m_2 \text{ erg s}^{-1}, \quad (27)$$

where  $\Gamma_b = 2\Gamma_2$ , and  $\xi = 0.1\xi_{0.1}$  is the radiative efficiency of the kinetic energy of the blob. This is consistent with the estimation from  $\Gamma_b^4 \xi E_{\text{BZ}}/t_{\text{rise}}$ , where  $E_{\text{BZ}}$  is the total energy pumped from the BH spin (see the Appendix). The rise luminosity is proportional to  $d\Delta M_{\text{BLR}}/dt \propto R_{\text{blob}}^2 n_{\text{BLR}} \propto t^{4/5}$  (swept by the transverse motion of the blob). After  $t_{\text{rise}}$ , the blob is significantly slowed down, and no significant fraction of the kinetic energy of the blob is converted into thermal energy for expansion, causing the radiation to decay. Considering that the luminosity radiated from the blob is from the expansion, we have  $L_{\text{obs}} \propto V_{\text{exp}}^2 \propto t^{-6/5}$ . We approximate the light curve as

$$L_{\text{obs}} = \begin{cases} L_{\text{peak}}^{\text{BZ}} (t/t_{\text{rise}})^{4/5} & (\text{for } t \lesssim t_{\text{rise}}), \\ L_{\text{peak}}^{\text{BZ}} (t/t_{\text{rise}})^{-6/5} & (\text{for } t \gtrsim t_{\text{rise}}). \end{cases} \quad (28)$$

After one GW burst, the AMS first forms an ejected blob through the BZ mechanism (mainly determined by  $t_a$ ), and then the ejected blob appears as a giant flare with rise and decay timescales of a few  $\times 10^6$  s. The EMC appears more than 10 days after the GW burst.

For a simple estimation of the spectral energy distribution, we follow the treatment in Wang et al. (2021). Relativistic electrons are produced by Fermi acceleration (Blandford & Eichler 1987) but lose their energy via synchrotron and inverse Compton (IC) scattering. The maximum Lorentz factor is given by the balance between the acceleration and radiation. Shocks from the Sedov expansion accelerate electrons to the relativistic regime, generating a flare of nonthermal radiation from radio to  $\gamma$ -ray energies. For a magnetic field in equipartition with the postshocked gas, we have  $B = 6.0(n_{\text{BLR},7} T_9)^{1/2}$  G, where  $T_9 = T/10^9$  K is the temperature of the postshocked gas. The maximum Lorentz factor of the electrons is determined by the balance between energy loss and gain. For a typical quasar with  $M_* = 10^8 M_{\odot}$  and  $\mathcal{M} = 1.0$ , the energy density of the radiation field is about  $u_{\text{ph}} = L_{\text{bol}}/4\pi R_{\text{BLR}}^2 c = 0.16 L_{45} R_{50}^{-2} \text{ erg cm}^{-3}$ , which peaks at UV frequencies of  $\nu_{\text{UV}} \sim 10^{15}$  Hz, where  $L_{45} = L_{\text{bol}}/10^{45} \text{ erg s}^{-1}$  and  $R_{50}$  is the BLR radius in units of 50 lt-days (Wang et al. 2021). We find  $u_{\text{ph}} \ll u_{\text{B}}$ , where  $u_{\text{B}} = B^2/8\pi$  is the energy density of magnetic fields; namely, synchrotron radiation dominates over IC. Taking the balance between the acceleration and synchrotron loss, we have the

maximum Lorentz factor of  $\gamma_{\text{max}} = 1.5 \times 10^6 (B/6 \text{ G})^{1/2} T_9^{1/2}$  at the peak time of luminosity. The synchrotron and IC luminosities are

$$\begin{aligned} L_{\text{syn}}^{\text{blob}} &= 1.6 \times 10^{45} \xi_{0.1} \Gamma_2^4 E_{51} t_{\text{rise},6}^{-1} \text{ erg s}^{-1}, \\ L_{\text{IC}}^{\text{blob}} &= 1.6 \times 10^{44} \Gamma_2^4 \left( \frac{u_{\text{ph}}/u_{\text{B}}}{0.1} \right) \left( \frac{L_{\text{syn}}^{\text{blob}}}{10^{44} \text{ erg s}^{-1}} \right) \text{ erg s}^{-1}, \end{aligned} \quad (29)$$

with the synchrotron and IC frequencies, respectively, where  $t_{\text{rise},6} = t_{\text{rise}}/10^6$  s,

$$\begin{aligned} \nu_{\text{syn}} &= 206.4 \left( \frac{B}{6 \text{ G}} \right) \Gamma_2 \gamma_{\text{max},6}^2 \text{ keV}, \\ \nu_{\text{IC}} &= 8.2 \Gamma_2 \gamma_{\text{max},6}^2 \nu_{\text{UV},15} \text{ TeV}, \end{aligned} \quad (30)$$

where  $\gamma_{\text{max},6} = \gamma_{\text{max}}/10^6$  and  $\nu_{\text{UV},15} = \nu_{\text{UV}}/10^{15}$  Hz. After the luminosity peak, the characteristic frequencies shift toward lower frequencies with time. The ejected blob will release energy over a wide range of frequencies from radio to TeV. It should be pointed out that all calculations for radiations are estimated in a rough rather than self-consistent way.

It should be noted that the BZ-powered EMC depends on a sufficiently high BH spin and accretion rate, which implies that the BZ mechanism does not work in type II AMSs. There is an absence of BZ-powered blobs in cases B and C.

### 3.3.2. Bondi Explosion

The huge energy accumulated from the hyper-Eddington accretion (Equation 16) during  $t_a$  will drive the Bondi explosion, which can be divided into three phases. As briefly discussed in Wang et al. (2021), internal shocks due to the collision between the outflows and the Bondi sphere efficiently dissipate kinetic energy into thermal energy. The Bondi sphere freely expands and then enters the blast wave and snowplow phases. We approximate its expansion velocity as

$$V_{\text{exp}} = \begin{cases} V_{\text{free}} \approx 3.2 \times 10^3 E_{52}^{1/2} M_{\text{Bon},2}^{-1/2} \text{ km s}^{-1} & (\text{for } t \lesssim t'_c), \\ V_{\text{Sedov}} = 3.2 \times 10^3 (t/t'_c)^{-3/5} \text{ km s}^{-1} & (\text{for } t \gtrsim t'_c), \end{cases} \quad (31)$$

where  $V_{\text{free}} = \sqrt{2E_{\text{out}}/M_{\text{Bon}}}$  is the free expansion velocity,  $t'_c \approx 4.0$  yr, and  $R'_c \approx 3.9 \times 10^{16}$  cm by setting the free expansion velocity equal to the velocity during the Sedov phase. The thermal emission of the Bondi sphere dominates at this moment ( $t'_c$ ) and ends the free expansion, and the optical depth of the Bondi sphere is  $\tau_{\text{es}}^0 \approx 3\kappa_{\text{es}} M_{\text{Bon}}/4\pi R'_c{}^2 = 21.9$  for  $M_{\text{Bon}} = 2.1 \times 10^2 M_{\odot}$  and  $R'_c = 3.9 \times 10^{16}$  cm. When the Bondi sphere becomes transparent, its thermal emission reaches the peak with the timescale of photon diffusion

$$t'_{\text{rise}} = \frac{\tau_{\text{es}}^0 R'_c}{c} = 0.92 \left( \frac{M_{\text{Bon},2}}{2.1} \right) \left( \frac{R'_{c,16}}{3.9} \right)^{-1} \text{ yr}, \quad (32)$$

where  $R'_{c,16} = R'_c/10^{16}$  cm, and the peak luminosity

$$L_{\text{Bon}} \approx \frac{E_{\text{out}}}{t'_{\text{rise}}} = 3.5 \times 10^{44} E_{52} \left( \frac{M_{\text{Bon},2}}{2.1} \right)^{-1} \left( \frac{R'_{c,16}}{3.9} \right) \text{ erg s}^{-1}. \quad (33)$$

Considering that blackbody radiation increases with the surface area of the sphere, the rise light curve is  $L_{\text{Bon}} \propto R_{\text{exp}}^2 \propto t^{4/5}$ . Meanwhile, the thermal energy decays with the expansion kinetic energy as  $L_{\text{Bon}} \propto V_{\text{exp}}^2 \propto t^{-6/5}$ . We approximate the light curve as

$$L_{\text{obs}} = \begin{cases} L_{\text{Bon}}(t/t'_{\text{rise}})^{4/5} & (\text{for } t \lesssim t'_{\text{rise}}), \\ L_{\text{Bon}}(t/t'_{\text{rise}})^{-6/5} & (\text{for } t \gtrsim t'_{\text{rise}}). \end{cases} \quad (34)$$

The characteristic temperature of the Bondi sphere peaks at

$$T_{\text{peak}} = \left( \frac{L_{\text{Bon}}}{4\pi\sigma_{\text{ST}}R_c'^2} \right)^{1/4} \approx 4200 \left( \frac{L_{\text{Bon},44}}{3.5} \right)^{1/4} \left( \frac{R_{c,16}'}{3.9} \right)^{-1/2} \text{ K}, \quad (35)$$

where  $\sigma_{\text{ST}} = 5.67 \times 10^{-5} \text{ erg s}^{-1} \text{ cm}^{-2} \text{ K}^{-4}$  is the Stefan–Boltzmann constant, and  $L_{\text{Bon},44} = L_{\text{Bon}}/10^{44} \text{ erg s}^{-1}$ . Moreover, the Bondi explosion may convert thermal energy into nonthermal energy through strong shocks when they pass through the BLR.

The Bondi sphere, as it expands with the Sedov velocity, generates shocks in the BLR. We approximate the magnetic field of the postshock gas as  $B = 1.9(n_{\text{BLR},7}T_8)^{1/2} \text{ G}$ , where  $T_8 = T/10^8 \text{ K}$ . In this case,  $u_B \approx u_{\text{ph}}$ . With a radiative efficiency  $\xi = 0.1$ , the nonthermal emission due to gas shocked by the Bondi explosion peaks at frequencies

$$\begin{aligned} \nu_{\text{syn}} &= 10.5 \left( \frac{B}{1.9 \text{ G}} \right) \left( \frac{\gamma_{\text{max},5}}{5.7} \right)^2 \text{ keV}, \\ \nu_{\text{IC}} &= 1.4 \left( \frac{\gamma_{\text{max},5}}{5.7} \right)^2 \nu_{\text{UV},15} \text{ TeV}, \end{aligned} \quad (36)$$

at a luminosity

$$L_{\text{syn}}^{\text{Bon}} \approx L_{\text{IC}}^{\text{Bon}} \approx 1.7 \times 10^{43} \xi_{0.1} E_{52}(t/t'_{\text{rise}})^{-1} \text{ erg s}^{-1}, \quad (37)$$

where  $\gamma_{\text{max},5} = \gamma_{\text{max}}/10^5$ . The synchrotron radiation is approximately equal to the IC, since  $u_B \approx u_{\text{ph}}$ . The peak luminosity in the X-rays may be marginally detectable when compared to the expected level of emission from the SMBH disk. Estimating the radio emission as a power law ( $L_\nu \propto \nu^{-0.5}$ ),  $L_{5 \text{ GHz}} \approx 10^{39} \text{ erg s}^{-1}$  at 5 GHz, which is comparable to the brightness of AGNs of moderate radio power (e.g., Elvis et al. 1994). The rise and decay light curves follow  $t^{4/5}$  and  $t^{-6/5}$ , respectively, which can be used as a diagnostic of the event from AGN light curves.

We note that Kimura et al. (2021) recently studied the evolution of BBHs formed in nuclear star clusters that are trapped by the SMBH disk. Their model depends on the in situ formation of BBHs in a nuclear star cluster, a scenario different from ours. We consider BBHs formed in the cavities of type I AMSs. The rejuvenation of AMSs due to Bondi accretion of BBHs efficiently removes the orbital AM of the binaries, leading to a merger event and a GW burst. Meanwhile, a Bondi explosion driven by the powerful outflows from the hyper-Eddington accretion onto the BBH gives rise to an EMC. Detailed numerical simulations have been done for the orbital evolution of BBHs in SMBH disks (Li et al. 2021), but they do not include outflows. In this paper, we omit detailed discussions of the accretion onto BBHs, such as in the

individual mini disks of each BH and the circumbinary disk (Kimura et al. 2021). Our discussions should be valid, since the timescale for forming the central cavity could be significantly longer than the characteristic timescales  $t_a$  and  $t_{\text{vis}}$ . Moreover, the initial separation of the BBH is much smaller than the Bondi radius. The behavior of Bondi–Hoyle–Lyttleton accretion onto BBHs (Antoni et al. 2019; Comerford et al. 2019) differs from the classical one (e.g., Artymowicz et al. 1993). A cavity around the BBH is, in principle, formed on a dynamical timescale when the disk around the BBH is geometrically thin, but the current case of hyper-Eddington accretion (geometrically thick) is more uncertain.

The present scenario of BZ-powered emission and a Bondi explosion could be a possible mechanism to drive AGN variability on timescales of months to years. The event rates depend on the number of BHs. Investigating AGN light curves requires continuous, long-term observational campaigns with suitable cadence in order to capture their rise and decay for comparison with theoretical predictions. Radiation from the AMS depends on its BH mass, locations, and the vertical structure of the SMBH disks. In the work of Perna et al. (2021) and Zhu et al. (2021), AMSs are located at  $10^3 R_g$ . Moreover, they consider the influence of the vertical structure of the SMBH disks on the AMSs of neutron stars. In future papers, we will test how the properties of AMSs change with location within the SMBH disk.

### 3.4. The Case of GW190521

We briefly apply the current model to explain the case of GW190521. This GW burst is a merger of  $85 + 66 M_\odot$  BHs, which are much higher than the upper limit of BHs produced by isolated massive stars driven by pair instability (e.g., Woosley et al. 2002). Our model of AMSs in SMBH disks provides a promising framework for stellar-mass BHs to rapidly grow to exceed the pair instability limit. For an exponentially growing AMS BH, we have  $m_* = m_*^0 \exp(\langle \dot{m}_* \rangle t / t_{\text{Salp}})$ , where  $m_*^0$  is the initial mass of the BH,  $\langle \dot{m}_* \rangle = \dot{m}_* \delta$  is the average rate of accretion onto the BH over time  $t$ ,  $\dot{m}_* = f_a \dot{m}_{\text{Bon}}$ ,  $f_a$  is the fraction of the accretion rate channeled into the outflow (Takeo et al. 2020; Wang et al. 2021), and  $t_{\text{Salp}} = m_*/\dot{M}_{\text{Edd}} = 0.45 \text{ Gyr}$  is the Salpeter time. The exponential growth reads

$$m_* = m_*^0 \exp \left[ 6 \left( \frac{\langle \dot{m}_* \rangle_6 t}{t_{\text{Salp}}} \right) \right] \approx 7.4 m_*^0 \quad (38)$$

for  $t = t_{\text{Salp}}/3$ , where  $\langle \dot{m}_* \rangle_6 = (\delta_6/6)\dot{m}_9 f_3$ ,  $\delta_6 = \delta_*/10^{-6}$ , and  $\dot{m}_9 = \dot{M}_{\text{Bon}}/10^9 \dot{M}_{\text{Edd}}$  for BHs with an initial mass of  $10 M_\odot$  (see Equation (20) in Wang et al. 2021). Most of the uncertainty in the growth rate derives from  $f_a$ , but it is easy for the BH to grow to  $\sim 10^2 M_\odot$  from  $10 M_\odot$  within one AGN lifetime ( $t = t_{\text{AGN}}$ ) in the context of SMBH disks.

Three kinds of EMCs with GW bursts have been suggested in Section 3.3. With  $m_* \approx 150 M_\odot$ , the characteristic of an EMC driven by the BZ-powered blob is generally consistent with the flare of the quasar SDSS J1249+3449 monitored by the Zwicky Transient Facility (Graham et al. 2020). Moreover, there is a delay of  $\sim 20$  days (in the quasar’s frame) of the EMC candidate (J1249+3449) with respect to GW190521. This can be conveniently explained by  $t_{\text{rise}}$  in the case of an ejected blob. We thus prefer case A of the EMC of GW190521 associated with the BZ-powered ejected blob, as shown in Figure 2. The

predicted thermal emission from the Bondi sphere and nonthermal emission from the Bondi explosion can be tested observationally, as explored in an upcoming work, and all calculations of radiations will be done in a self-consistent way.

#### 4. Discussion and Conclusions

Compact objects (neutron stars and stellar-mass BHs) manifest themselves as AMSs in the accretion disks of SMBHs (SMBH disks) in AGNs. The AMSs around stellar-mass BHs fall into two classes: cold gas-enshrouded type I and hot gas-enshrouded type II. This paper studies the dynamics of both classes in the context of SMBH disks. We show that most AMSs dynamically evolve into tight BBHs. The BBH evolves under the tidal torque of the central SMBH until it rejuvenates by hot gas accretion during the type II phase. We show that the orbital AM of the BBH is efficiently removed by the gaseous drag during the initial type I phase. With an onset separation of  $\sim 10^2 r_g$  in this phase, the subsequent release of GW radiation leads to the merger of the BBH after  $\sim 3$  hr. The GW burst rate in a typical quasar is estimated to be  $3.2 \times 10^{-3} \text{ yr}^{-1}$  if we conservatively assume that the SMBH disk contains  $N_s = 40$  BHs with  $10^2 M_\odot$ . The predicted GW frequency of  $\sim 10^2$  Hz is accessible by LIGO. Considering the entire quasar population at  $z \lesssim 1$ , the rate of GW bursts from AMS binaries is expected to be  $\sim 3 \text{ yr}^{-1}$ . The binary formation rates given by Equation (11) are significantly higher than the tidal disruption rates of stars ( $\sim 10^{-4} \text{ yr}^{-1}$ , depending on the SMBH mass in galactic centers; see details in Wang & Merritt 2004). However, GW rates depend on the number of BHs, which is currently poorly known. Since the orbit evolution is much shorter than the typical lifetime of AGNs, the binary formation rate can be traced by AGN flares. Detection of  $\sim 10^2$  Hz GWs will reveal the content of stellar BHs in SMBH disks.

Three kinds of EMCs of GW bursts are predicted, driven by the BZ mechanism or a Bondi explosion from powerful outflows. The BZ-powered EMCs with mildly relativistic motion appear from radio to TeV bands with a rise time of a few  $10^6$  s and decay with  $t^{-6/5}$ . Bondi spheres have thermal emission peaking in the optical, and the Bondi explosion driven by powerful outflows has detectable nonthermal emissions from radio to  $\gamma$ -rays. The EMCs have a rise profile of  $t^{4/5}$  and decay with  $t^{-6/5}$ . Depending on the viscosity of the Bondi sphere, the EMCs could appear in three ways. An efficient viscosity results in a GW burst to lead the EMCs, but an inefficient viscosity postpones BBH to merge, with the result that Bondi explosion leads as a precursor of GW bursts. A moderate viscosity may lead to a simultaneous appearance of GW bursts and EMCs, but the EMCs will have a much longer duration. A search for these flares from radio to  $\gamma$ -rays in AGNs and quasars using the Zwicky Transient Facility, Swift, and Fermi observations will advance the understanding of the physics currently discussed. There is the potential to simultaneously detect GW bursts corresponding to EMCs.

We stress that the GW bursts should be redshifted or blueshifted if detected by LIGO because the BBH corotates with and merges within the SMBH disk. The characteristic shifts would be  $\sim \pm 3000 r_4^{-1/2} \text{ km s}^{-1}$ , depending on the direction of motion of the BBH with respect to the observer and its distance to the SMBH. These are pure Doppler shifts. Moreover, gravitational redshifts could also arise if the BBH merges close enough to the SMBH (e.g., Chen et al. 2019). The Doppler and gravitational redshifts of GW bursts are important diagnostics to probe their birthplace: the SMBH disk. Lastly, we note that the BBHs and SMBH comprise another binary

(with an extreme mass ratio inspiral of  $\sim 10^{-7}$ ) and radiate GWs with frequencies of  $f \sim 0.64 M_8^{-1} r_4^{-3/2} \text{ nHz}$ , which is only detectable through pulsar timing arrays.

The authors are grateful to an anonymous referee for a useful report that clarified several points in this paper. Useful discussions are acknowledged with members of the IHEP AGN Group. We are thankful for the support from the National Key R&D Program of China (2016YFA0400701, 2016YFA0400702, 2020YFC2201400), NSFC (NSFC-11991050, -11991054, -11833008, -11721303, -11991052, -11690024, QYZDJ-SSW-SLH007, XDB23010400), and the International Partnership Program of the Chinese Academy of Sciences (113111KYSB20200014). We acknowledge the science research grants from the China Manned Space Project with NO.CMS-CSST-2021-B11.

#### Appendix

##### BZ-powered Jets from Hyper-Eddington Accretion

The BZ mechanism is a powerful process of pumping energy from the BH spin (Blandford & Znajek 1977). Given a BH with a spin AM  $\mathcal{J}$  and magnetic field  $B$  normal to the horizon at  $R_h$ , the pumping power is given by Macdonald & Thorne (1982) and Ghosh & Abramowicz (1997),

$$L_{\text{BZ}} = \left( \frac{1}{32} \right) \omega_F^2 B_\perp^2 R_h^2 c \left( \frac{\mathcal{J}}{\mathcal{J}_{\text{max}}} \right)^2, \quad (\text{A1})$$

where  $\mathcal{J}_{\text{max}}$  is the maximum of the spin AM, and  $\omega_F = \Omega_F(\Omega_h - \Omega_F)/\Omega_h^2$  is the factor describing the relative angular velocity of the magnetic field to the BH ( $\Omega_h$ ). The BZ power has been calculated by Armitage & Natarajan (1999) for optically thin advection-dominated accretion flows. Following this treatment, we use the self-similar solution of super-Eddington accretion (Wang & Zhou 1999) for the energy channeled into a relativistic jet. We take the magnetic field of  $B_\perp^2/8\pi = \alpha P_{\text{rad}}$  (in equipartition with the radiation field) and  $R_h = Gm_*/c^2$ , where  $P_{\text{rad}} = \dot{M}_{\text{Bon}} \Omega_K/4\pi\alpha R$  is the radiation pressure of the super-Eddington accretion (dominated by gas pressure). Here we stress that the accretion rate of the BH  $\dot{M} = f_a \dot{M}_{\text{Bon}}$  is only a small fraction of the Bondi rate, and the factor  $f_a$  is uncertain (see the latest simulations of Takeo et al. 2020). For a maximally rotating BH, the BZ power

$$L_{\text{BZ}} \approx \left( \frac{1}{64} \right) \dot{M} c^2 = 2.0 \times 10^{45} f_3 \dot{m}_{10} m_2 \text{ erg s}^{-1}, \quad (\text{A2})$$

with  $\omega_F = 1/2$  as taken by Armitage & Natarajan (1999), and the total pumped energy during the hyper-Eddington accretion episode ( $t_a$ ) is given by

$$E_{\text{BZ}} = L_{\text{BZ}} t_a = 2 \times 10^{51} f_3 \dot{m}_{10} m_2 t_{a,6} \text{ erg}, \quad (\text{A3})$$

where  $f_3 = f_a/10^{-3}$  and  $t_{a,6} = t_a/10^6$  s. Chen & Zhang (2021) recently expressed the BZ-powered jet in an approximate analytical form. We take the outermost magnetic stream surface as the radius of the jet from their Equation (105),

$$R_{\text{jet}} = C_2^{-1/2} (1 + \sqrt{1 - a^2})^{\nu/2} \left( \frac{z}{r_g} \right)^{1-\nu/2} \\ r_g = 1.7 \times 10^{12} R_{\text{Bon},15}^{5/8} m_2^{3/8} \text{ cm}, \quad (\text{A4})$$

where  $C_2 = \Gamma(3/2 - \nu/2)\Gamma(1 + \nu/2)/\sqrt{\pi}$  is a constant,  $\Gamma$  is the  $\Gamma$  function, and  $\nu$  is the power index of the magnetic fields along the AMS radius. For a typical value of  $\nu = 3/4$ ,  $C_2 = 0.47$ . The jet or ejecta are choked by the dense medium of the SMBH disk (e.g., Matzner 2003; Zhu et al. 2021) to form a blob moving with a mildly relativistic velocity.

### ORCID iDs

Jian-Min Wang  <https://orcid.org/0000-0001-9449-9268>

Luis C. Ho  <https://orcid.org/0000-0001-6947-5846>

Yan-Rong Li  <https://orcid.org/0000-0001-5841-9179>

Pu Du  <https://orcid.org/0000-0002-5830-3544>

### References

- Abbott, B. P., Abbott, R., Abbott, T. D., et al. 2016a, *PhRvL*, **116**, 061102
- Abbott, B. P., Abbott, R., Abbott, T. D., et al. 2016b, *PhRvL*, **116**, 241103
- Abbott, B. P., Abbott, R., Abbott, T. D., et al. 2017, *PhRvL*, **118**, 221101
- Abbott, R., Abbott, T. D., Abraham, S., et al. 2020, *PhRvL*, **125**, 1102
- Abramowicz, A., Czerny, B., Lasota, J.-P., & Szuszkiewicz, E. 1988, *ApJ*, **332**, 646
- Antoni, A., MacLeod, M., & Ramirez-Ruiz, E. 2019, *ApJ*, **884**, 22
- Antonini, F., & Perets, H. B. 2012, *ApJ*, **757**, 27
- Arcodia, R., Merloni, A., Nandra, K., et al. 2021, *Natur*, **592**, 704
- Armitage, P. J., & Natarajan, P. 1999, *ApJL*, **523**, L7
- Artymowicz, P., Lin, D., & Wampler, E. J. 1993, *ApJ*, **409**, 592
- Bartos, I., Kocsis, B., Haiman, Z., et al. 2017, *ApJ*, **835**, 165
- Blandford, R., & Eichler, D. 1987, *PhR*, **154**, 1
- Blandford, R. D., & Znajek, R. L. 1977, *MNRAS*, **179**, 433
- Bondi, H. 1952, *MNRAS*, **112**, 195
- Bromberg, O., Nakar, E., Piran, T., et al. 2011, *ApJ*, **740**, 100
- Cantiello, M., Jermyn, A. S., & Lin, D. N. C. 2021, *ApJ*, **910**, 94
- Chen, L., & Zhang, B. 2021, *ApJ*, **906**, 105
- Chen, X., Li, S., & Cao, Z. 2019, *MNRAS*, **485**, L141
- Cheng, K. S., & Wang, J.-M. 1999, *ApJ*, **521**, 502
- Collin, S., & Zahn, J.-P. 1999, *A&A*, **344**, 433
- Collin, S., & Zahn, J.-P. 2008, *A&A*, **477**, 419
- Comerford, T. A. F., Izzard, R. G., Booth, R. A., & Rosotti, G. 2019, *MNRAS*, **490**, 5196
- Du, P., & Wang, J.-M. 2014, *MNRAS*, **438**, 2828
- Elvis, M., Wilkes, B. J., McDowell, J. C., et al. 1994, *ApJS*, **95**, 1
- Fender, R. P., Belloni, T. M., & Gallo, E. 2004, *MNRAS*, **355**, 1105
- Ghosh, P., & Abramowicz, M. 1997, *MNRAS*, **292**, 887
- Goodman, J. 2003, *MNRAS*, **339**, 937
- Goodman, J., & Tan, J. C. 2004, *ApJ*, **608**, 108
- Graham, M. J., Ford, K. E. S., McKernan, B., et al. 2020, *PhRvL*, **124**, 251102
- Grishin, E., Bobrick, A., Hirai, R., et al. 2021, *MNRAS*, in press (doi:10.1093/mnras/stab197)
- Gröbner, M., Ishibashi, W., Tiwari, S., et al. 2020, *A&A*, **638**, A119
- Hamann, F., & Ferland, G. 1999, *ARA&A*, **37**, 487
- Ho, L. C. 2002, *ApJ*, **564**, 120
- Ho, L. C. 2008, *ARA&A*, **46**, 475
- Hughes, S. A., & Blandford, R. 2003, *ApJL*, **585**, L101
- Kaaz, N., Schroder, S. L., Andrews, J. J., et al. 2021, *ApJ*, arXiv:2103.12088
- Kato, S., Fukue, J., & Mineshige, S. 2008, Black-hole Accretion Disks, Kyoto (Kyoto Univ. Press)
- Kimura, S. S., Muraes, K., & Bartos, I. 2021, arXiv:2103.02461
- Kitaki, T., Mineshige, S., Ohsuga, K., & Kawashima, T. 2018, *PASJ*, **70**, 108
- Kolykhalov, P. I., & Sunyaev, R. A. 1980, *SvAL*, **6**, 357
- Li, Y.-P., Dempsey, A. M., Li, S., et al. 2021, *ApJ*, **911**, 124
- LIGO Scientific Collaboration & Virgo Collaboration 2019a, *ApJL*, **882**, L24
- LIGO Scientific Collaboration & Virgo Collaboration 2019b, *PhRvX*, **9**, 031040
- Macdonald, D., & Thorne, K. S. 1982, *MNRAS*, **198**, 345
- Martinez, M. A. S., Fragione, G., Kremer, K., et al. 2020, *ApJ*, **903**, 67
- Matzner, C. D. 2003, *MNRAS*, **345**, 575
- McKernan, B., Ford, K. E. S., Bartos, I., et al. 2019, *ApJL*, **884**, L50
- McKernan, B., Ford, K. E. S., & O’Shaughnessy, R. 2020, *MNRAS*, **498**, 4088
- Milosavljević, M., Bromm, V., Couch, S. M., et al. 2009b, *ApJ*, **698**, 766
- Milosavljević, M., Couch, S. M., & Bromm, V. 2009a, *ApJL*, **696**, 146
- Moranchel-Basurto, A., et al. 2021, *ApJ*, **906**, 15
- Nagao, T., Maiolino, R., & Marconi, A. 2006, *A&A*, **447**, 863
- Naoz, S. 2016, *ARA&A*, **54**, 441
- Narayan, R., & Yi, I. 1994, *ApJ*, **428**, L13
- Ohsuga, K., Mori, M., Nakamoto, T., & Mineshige, S. 2005, *ApJ*, **628**, 368
- Paczynski, B. 1978, *AcA*, **28**, 91
- Palmese, A., Fishbach, M., Burke, C. J., Annis, J. T., & Liu, X. 2021, *ApJL*, **914**, L34
- Perna, R., Lazzati, D., & Cantiello, M. 2021, *ApJL*, **906**, L7
- Peters, P. C. 1964, *PhRv*, **136**, 1224
- Petruk, O., Kuzyo, T., Orlando, S., et al. 2021, *MNRAS*, **505**, 755
- Popham, R., Woosley, S. E., & Fryer, C. 1999, *ApJ*, **518**, 356
- Rees, M. J. 1988, *Natur*, **333**, 523
- Richards, G. T., Strauss, M. A., Fan, X., et al. 2006, *AJ*, **131**, 2766
- Sadowski, A., & Narayan, R. 2015, *MNRAS*, **453**, 3213
- Sadowski, A., & Narayan, R. 2016, *MNRAS*, **456**, 3929
- Samsing, J., Bartos, I., D’Orazio, D. J., et al. 2020, arXiv:2010.09765
- Secunda, A., Bellovary, J., Mac Low, M.-M., et al. 2020, *ApJ*, **903**, 133
- Shakura, N. I., & Sunyaev, R. A. 1973, *A&A*, **24**, 337
- Shin, J., Woo, J.-H., Nagao, T., et al. 2013, *ApJ*, **763**, 58
- Shlosman, I., & Begelman, M. C. 1989, *ApJ*, **341**, 685
- Sikora, M., Stawarz, L., & Lasota, J.-P. 2007, *ApJ*, **658**, 815
- Takeo, E., Inayoshi, K., & Mineshige, S. 2020, *MNRAS*, **497**, 302
- Tanaga, H., Haiman, Z., & Kocsis, B. 2020, *ApJ*, **898**, 25
- Thorne, K. S., & Żytkow, A. N. 1975, *ApJL*, **199**, L19
- Thorne, K. S., & Żytkow, A. N. 1977, *ApJ*, **212**, 832
- Toomre, A. 1964, *ApJ*, **139**, 1217
- Wang, J., & Merritt, D. 2004, *ApJ*, **600**, 149
- Wang, J.-M., Chen, Y.-M., & Hu, C. 2006, *ApJ*, **637**, L85
- Wang, J.-M., Du, P., Baldwin, J. A., et al. 2012, *ApJ*, **746**, 137
- Wang, J.-M., Ge, J.-Q., Hu, C., et al. 2011, *ApJ*, **739**, 3
- Wang, J.-M., Liu, J.-R., Ho, L. C., & Du, P. 2021, *ApJL*, **911**, L14
- Wang, J.-M., Yan, C.-S., Gao, H.-Q., et al. 2010, *ApJL*, **719**, L148
- Wang, J.-M., & Zhou, Y.-Y. 1999, *ApJ*, **516**, 420
- Warner, C., Hamann, F., & Dietrich, M. 2003, *ApJ*, **596**, 72
- Woosley, S. E. 1993, *ApJ*, **405**, 273
- Woosley, S. E., Heger, A., & Weaver, T. A. 2002, *RvMP*, **74**, 1015
- Yang, Y., Bartos, I., Gayathri, V., et al. 2019, *PhRvL*, **123**, 181101
- Yang, Y., Gayathri, V., Bartos, I., et al. 2020, *ApJL*, **901**, L34
- Zhu, J.-P., Zhang, B., Yu, Y.-W., et al. 2021, *ApJL*, **906**, L11